Supporting Information:

Metal-Organic Framework-Derived Co_3ZnC/Co Embedded in Nitrogen-Doped Carbon Nanotube-Grafted Carbon Polyhedra as a High-Performance Electrocatalyst for Water Splitting

Zhou Yu,[†, ‡] Yu Bai, [*, ‡, §] Shimin Zhang, [†] Yuxuan Liu, [†] Naiqing Zhang, [‡] Guohua Wang, [‖] Junhua Wei, [‖] Qibing Wu, [‖] and Kening Sun, [*, ‡]

[†]School of Chemistry and Chemical Engineering and [‡]Academy of Fundamental and Interdisciplinary Sciences, Harbin Institute of Technology, Harbin 150090, P. R. China

[§]Advanced Research Institute for Multidisciplinary Science, Beijing Institute of Technology, Beijing 100081, P. R. China

[‖]State Key Laboratory of Advanced Chemical Power Sources, Zunyi 563000, P. R. China

*E-mail: yubaiit@163.com (Y. B).

*E-mail: keningsunhit@126.com (K. S.).

1 Experimental

1.1 Synthesis of ZnCo-ZIFs and ZIF-67.

All the chemicals were directly used after purchase without further purification. In a typical preparation, 4 mmol $Co(NO_3)_2{\cdot}6H_2O$ and 2 mmol $Zn(NO_3)_2{\cdot}6H_2O$ were dissolved into 40 mL of methanol (MeOH) and solution was then added into 30 mL of MeOH containing 24 mmol 2-methylimidazole (MeIM) under string. The mixed solution was placed at 25 °C for 24 h. The as-obtained powders were centrifuged with ethanol and dried in vacuum overnight to obtain the ZnCo-ZIFs. The preparation of ZIF-67 was performed with a similar process to ZnCo-ZIFs in the absence of $Zn(NO_3)_2{\cdot}6H_2O$.

1.2 Synthesis of Co_3ZnC/Co-NCCP, Co-NCCP and Co_3ZnC/Co-NCP.

The as-prepared ZnCo-ZIFs precursors were placed in a ceramic boat, and then heated in a tube furnace at a ramp rate of 5 °C/min to 600 °C under Ar/H_2 flow (95%/5% in volume ratio) for 1 h. After cooling naturally, the black product was finally collected. The Co-NCCP was obtained by treating ZIF-67 in the similar chemical vapor reduction and deposition process. The same procedure was conducted to convert ZnCo-ZIFs to Co_3ZnC/Co-NCP by calcination under Ar atmosphere.

1.3 Characterization.

Field emission scanning electron microscopy (FESEM) images were obtained on a Hitachi S-8010 scanning electron microscope. Transmission electron microscopy (TEM), high-resolution TEM (HRTEM), and energy-dispersive X-ray (EDX) elemental mapping images were all recorded on a FEI Tecnai G2 F30 (200 kV) high-resolution transmission electron microscope. X-ray diffraction (XRD) characterization was carried out on a PANalytical X'Pert PRO with Cu Ka radiation. X-ray photoelectron spectra (XPS) were obtained with a K-Alpha electron spectrometer (Thermofish Scientific Company) using Al Kα (1486.6 eV) radiation. The surface area was measured by the Brunauer-Emmett-Teller (BET) method using ASAP2020.

1.4 Electrochemical test.

Electrocatalytic activity evaluations were performed in a O_2-purged within the solution of 1 M KOH with a three-electrode system. The glassy carbon (GC) electrode (3 mm diameter) was utilized as the working electrode. The saturated Ag/AgCl electrode (SCE) was used as the reference electrode, and Pt mesh or a graphite electrode was used as the counter electrode. 2 mg sample was dispersed in 500 μL Nafion (5 wt%) -water-isopropyl alcohol mixture solution with a volume ratio of 0.05 : 4 : 1 by sonicating. Then, 6 μL of the dispersion was deposited onto a GC and dried in air overnight (loading ~0.21 mg cm^{-2}). The linear sweep voltammetry (LSV) was measured at 5 mV s^{-1} scanning rate. All the applied potentials were referenced to a reversible hydrogen electrode (RHE) scale. The long-term durability test was performed using chronoamperometry measurements. Electrochemical impendence spectroscopy (EIS) measurement was carried out from 0.1 Hz to 100 kHz at an overpotential of 300 mV. Cyclic voltammograms (CVs) were measured from 0.20 to 0.30 V *vs*. Ag/AgCl at scanning rates of 5, 10, 20, 40, 60, 80 and 100 mV s^{-1}. The overall water splitting performance was conducted using carbon cloth (1×1 cm) was utilized as working electrode to reach a high catalyst loading (1 mg cm^{-2}). For comparison, the same amount of noble metal catalysts, i.e., platinum/carbon (Pt/C) and RuO_2 were also supported on the carbon cloth as cathode and anode, respectively, to drive the overall water splitting process.

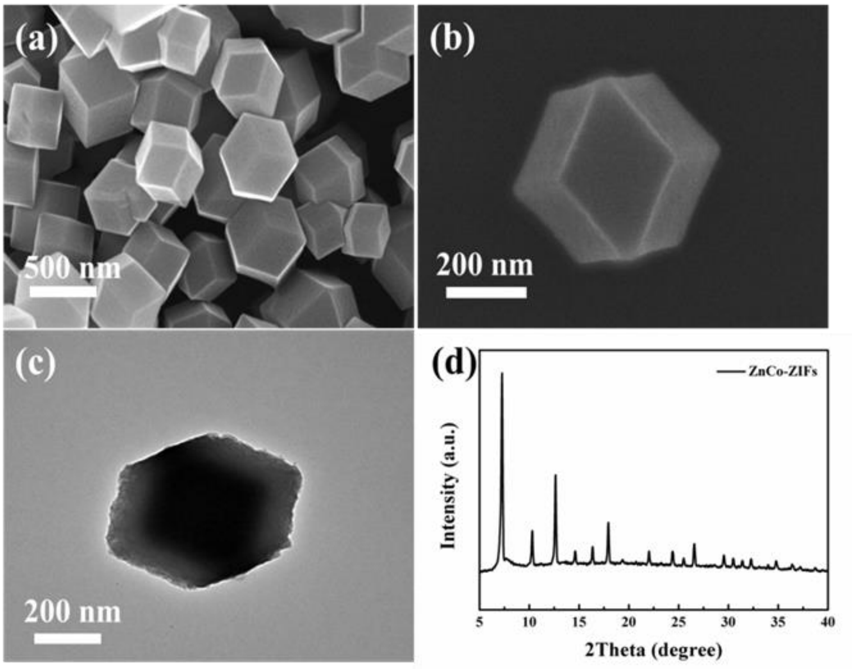

Fig. S1 (a, b) SEM images, (c) TEM images and (d) XRD patterns of ZnCo-ZIFs.

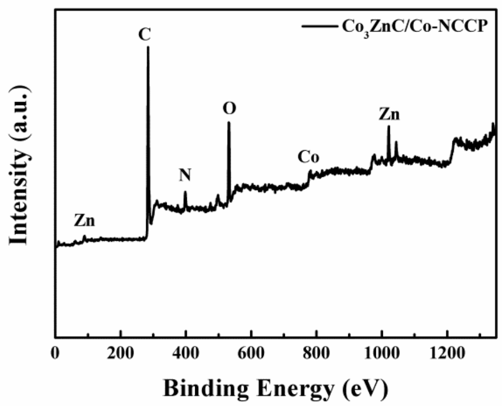

Fig. S2 Full scan XPS spectrum of Co_3ZnC/Co-NCCP.

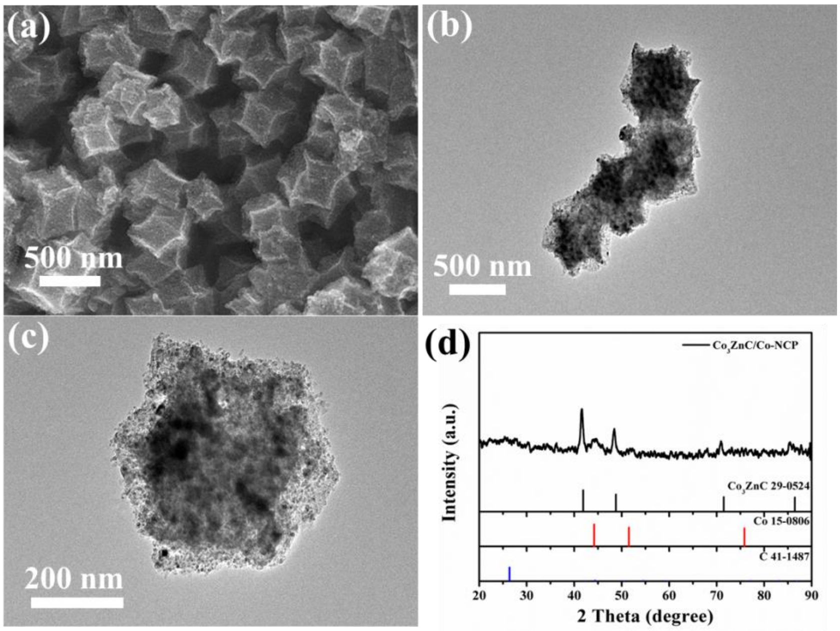

Fig. S3 (a, b) SEM, (c) TEM images and (d) XRD pattern of Co_3ZnC/Co-NCP.

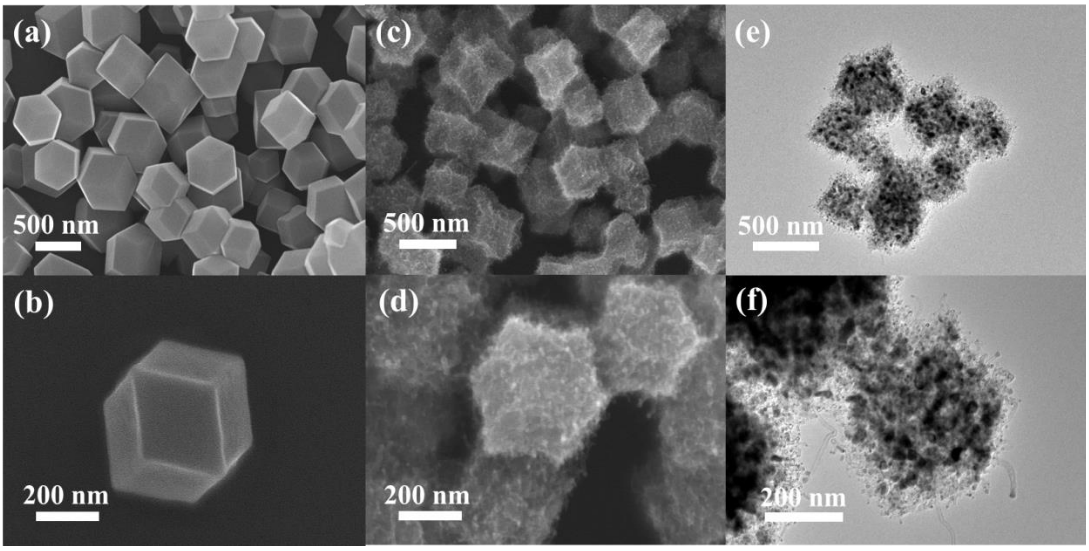

Fig. S4 (a) SEM and (b) TEM images of ZIF-67, (c, d) SEM images and (e, f) TEM images of Co-NCCP.

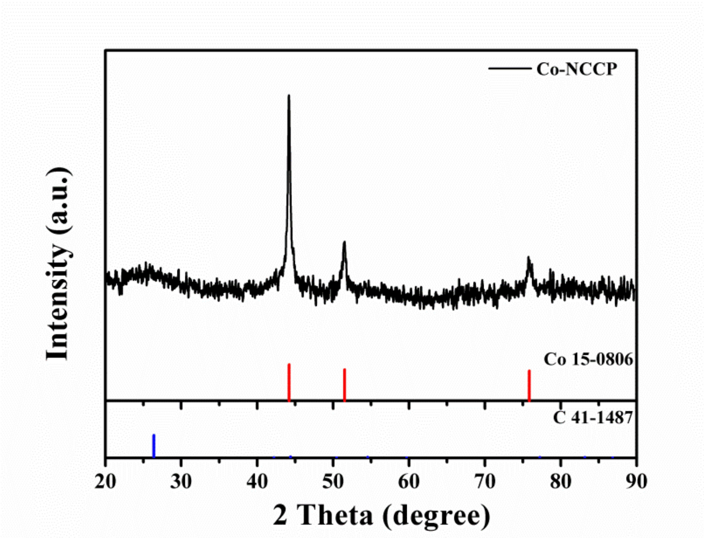

Fig. S5 XRD patterns of Co-NCCP.

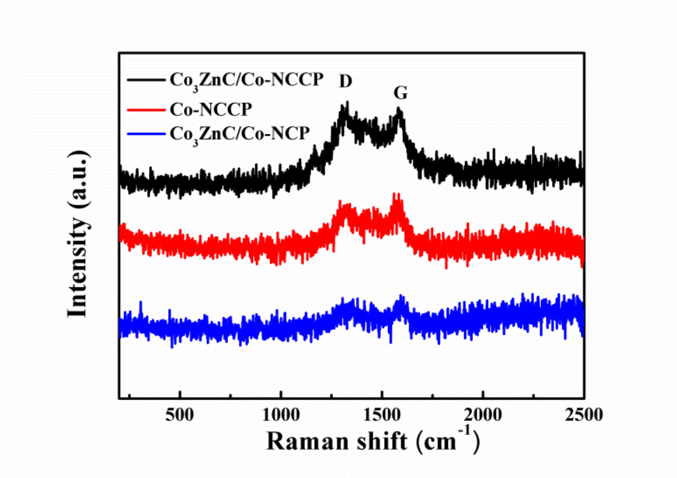

Fig. S6 Raman spectra of Co_3ZnC/Co-NCCP, Co-NCCP and Co_3ZnC/Co-NCP.

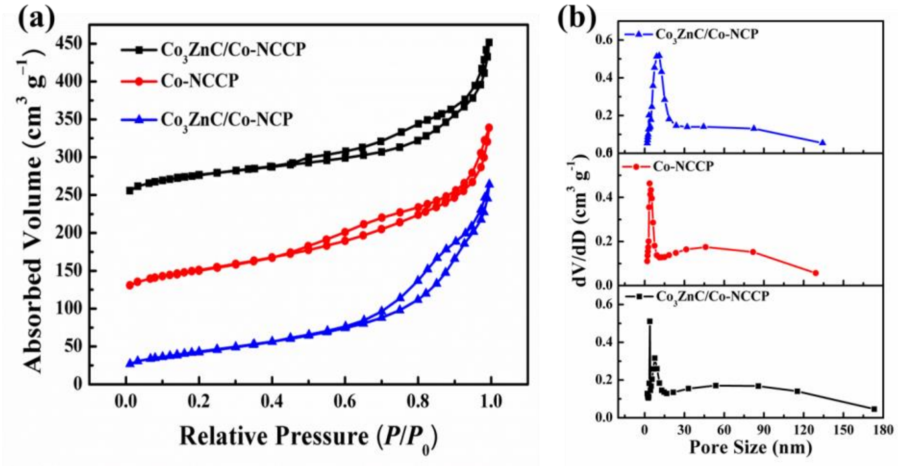

Fig. S7 (a) Nitrogen adsorption–desorption isotherm, and (b) BJH pore size distribution of Co_3ZnC/Co-NCCP, Co-NCCP and Co_3ZnC/Co-NCP.

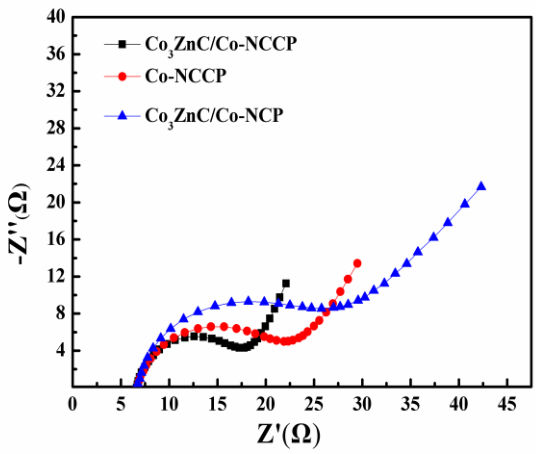

Fig. S8 Nyquist plots for Co_3ZnC/Co-NCCP, Co-NCCP and Co_3ZnC/Co-NCP in 1M KOH.

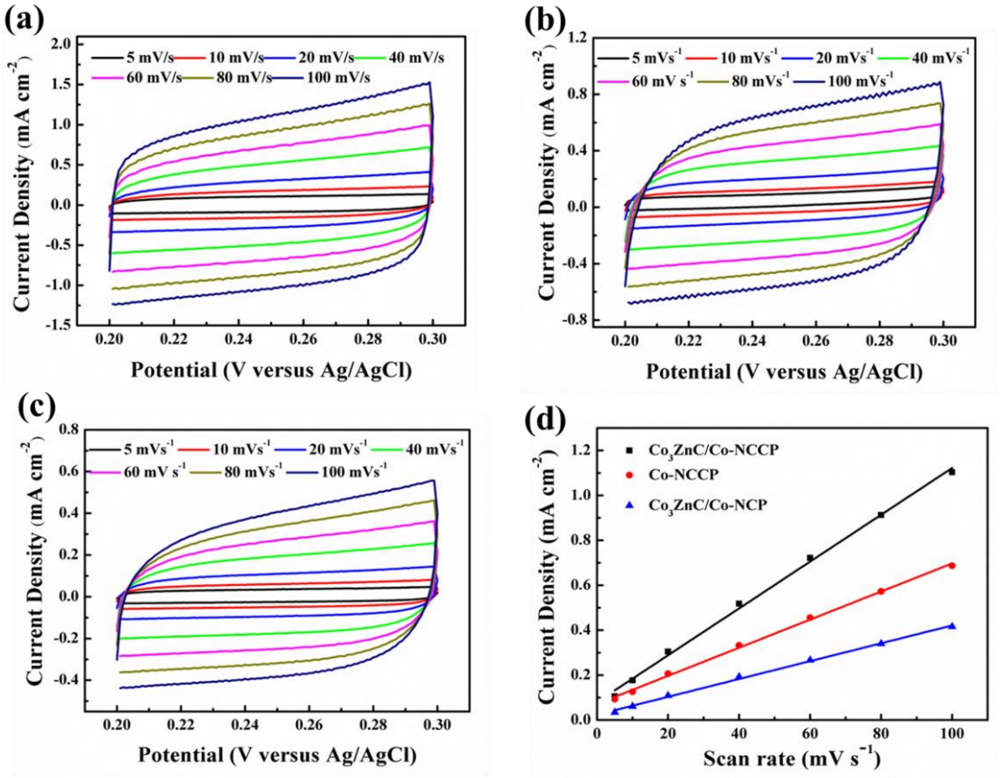

Fig. S9 Cyclic voltammograms in the double-layer region of the electrodes loaded with (a) Co_3ZnC/Co-NCCP, (b) Co-NCCP, and (c) Co_3ZnC/Co-NCP. (d) Current density *vs*. scan rate plot at 0.25 V.

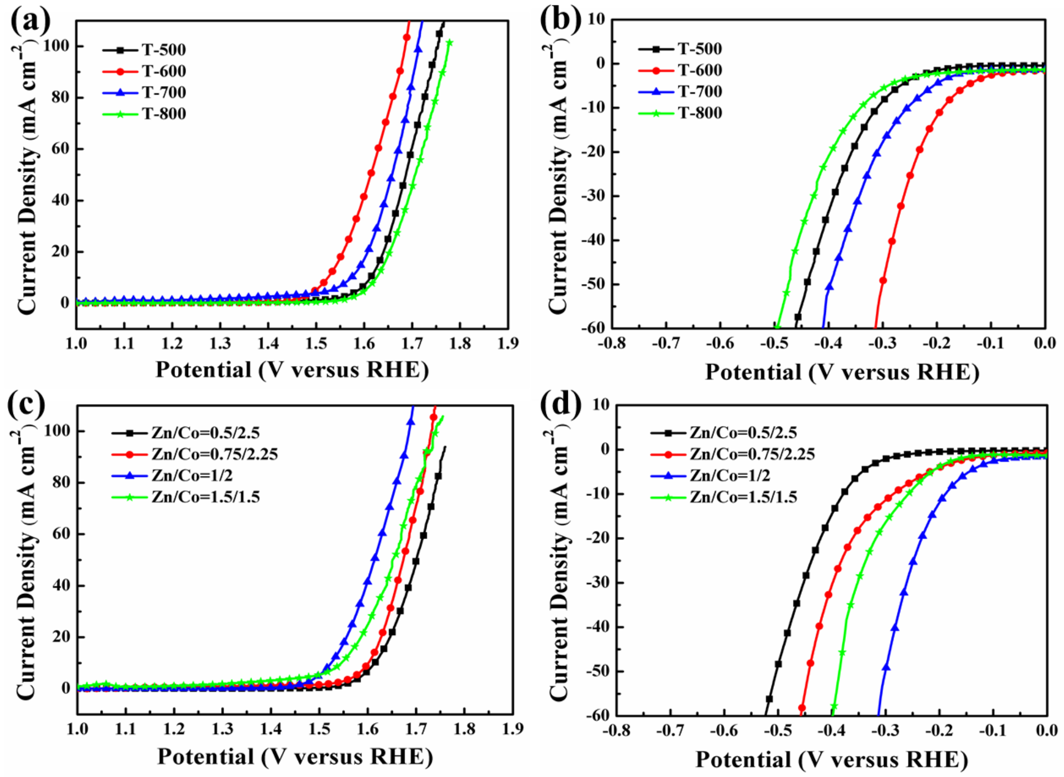

Fig. S10 (a) and (b) LSV curves of samples obtained at different sintering temperatures in 1M KOH. (c) and (d) LSV curves of samples prepared with different Zn/Co molar ratios in precursor.

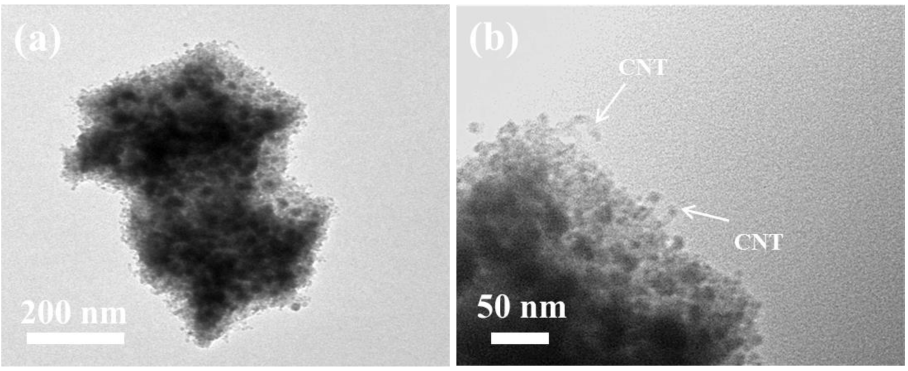

Fig. S11 (a, b) TEM image of Co_3ZnC/Co-NCCP after 10 h of electrolysis in 1M KOH .

Table S1. Comparison of electrochemical parameters of Co_3ZnC/Co-NCCP with the reported various OER catalysts in alkaline.

Electrocatalysts	**Overpotential (mV *vs*. RHE) at10 mA·cm^{-2}**	**Tafel slope**	**Electrolyte**	**Ref**
Co_3ZnC/Co-NCCP	295 mV	70 mV dec^{-1}	1 M KOH	This work
$Ni_3ZnC_{0.7}$-550	320 mV	52 mV dec^{-1}	1 M KOH	S1
Co-Mo-C/NRGO	330 mV	44 mV dec^{-1}	1 M KOH	S2
Co_3ZnC/Co@CN	366 mV	81 mV dec^{-1}	1 M KOH	S3
Fe_3C@NG800-0.2	361 mV	62 mV dec^{-1}	0.1 M KOH	S4
Co-NC/CNT	354 mV	78 mV dec^{-1}	1M KOH	S5
Ni/Mo_2C	368 mV	----	1 M KOH	S6
Co@Co_3O_4-NC	391 mV	102 mV dec^{-1}	1 M KOH	S7

Table S2. Comparison of electrochemical parameters of Co_3ZnC/Co-NCCP with the reported various HER catalysts in alkaline.

Electrocatalysts	**Overpotential (mV *vs*. RHE) at10 mA·cm^{-2}**	**Tafel slope**	**Electrolyte**	**Ref**
Co_3ZnC/Co-NCCP	188 mV	108 mV dec^{-1}	1 M KOH	This work
CoO_x@CN	232 mV	115 mV dec^{-1}	1 M KOH	S8
NiFe HNSs	189 mV	78.2 mV dec^{-1}	1 M KOH	S9
PNC/Co	298 mV	131 mV dec^{-1}	1 M KOH	S10
Co-NC/CNT	203 mV	125 mV dec^{-1}	1 M KOH	S11
$Co_{0.85}Se$@NC	230 mV	125 mV dec^{-1}	1M KOH	S12
CP/CTs/Co-S	190 mV	131 mV dec^{-1}	1 M KOH	S13
Ni/NC	219 mV	101 mV dec^{-1}	1 M KOH	S14

REFERENCES

[S1] Wang, Y.; Wu, W. T.; Rao, Y. Z.; Li, T.; Tsubaki, N.; Wu, M. B. Cation Modulating Electrocatalyst Derived from Bimetallic Metal-Organic Frameworks for Overall Water Splitting. *J. Mater. Chem. A* 2017, 5, 6170-6177.

[S2] Lan, Y. Q.; Liu, C. H.; Tang, Y. J.; Wang, X. L.; Huang, W.; Li, S. L.; Dong, L. Z. Highly Active Co-Mo-C/NRGO Composite as Efficient Oxygen Electrode for Water-Oxygen Redox Cycle. *J. Mater. Chem. A* 2016, 4, 18100-18106.

[S3] Su, J.; Xia, G.; Li, R.; Yang, Y.; Chen, J.; Shi, R.; Jiang, P.; Chen, Q. Co_3 ZnC/Co Nano-Heterojunctions Encapsulated in Nitrogen-Doped Graphene Layers

Derived from PBAs as Highly Efficient bi-functional Electrocatalysts for both OER and ORR. *J. Mater. Chem. A* 2016, 4, 9204-9212.

[S4] Jiang, H.; Yao, Y.; Zhu, Y.; Liu, Y.; Su, Y.; Yang, X.; Li, C. Iron Carbide Nanoparticles Encapsulated in Mesoporous Fe-N-Doped Graphene-Like Carbon Hybrids as Efficient Bifunctional Oxygen Electrocatalysts. *ACS Appl. Mater. Interfaces* 2015, 7, 21511-21520.

[S5] Yang, F. L.; Zhao, P. P.; Hua, X.; Luo, W.; Cheng, G. Z.; Xing, W.; Chen, S. L. A Cobalt-based Hybrid Electrocatalyst Derived from a Carbon Nanotube Inserted Metal-Organic Framework for Efficient Water-Splitting. *J. Mater. Chem. A* 2016, 4, 16057-16063

[S6] Yu, Z. Y.; Duan, Y.; Gao, M. R.; Lang, C. C.; Zheng, Y. R.; Yu, S. H. A One-dimensional Porous Carbon-Supported Ni/Mo_2C Dual Catalyst for Efficient Water Splitting. *Chem. Sci.* 2017, 8, 968-973

[S7] Bai, C. D.; Wei, S. S.; Deng, D. R.; Lin, X. D.; Zheng, M. S.; Dong, Q. F. A Nitrogen-doped Nano Carbon Dodecahedron with Co@Co_3O_4 Implants as Bi-functional Electrocatalyst for Efficient Overall Water Splitting. *J. Mater. Chem. A* 2017, 5, 9533-9536.

[S8] Jin, H.; Wang, J.; Su, D.; Wei, Z.; Pang, Z.; Wang, Y. In Situ Cobalt-Cobalt Oxide/N-doped Carbon Hybrids as Superior Bifunctional Electrocatalysts for Hydrogen and Oxygen Evolution. *J. Am. Chem. Soc.* 2015, 137, 2688-2694.

[S9] Sun, X. H.; Shao, Q.; Pi, Y.; Guo, J.; Huang, X. Q. A General Approach to Synthesis Ultrathin NiM (M=Fe, Co, Mn) Hydroxide Nanosheets as High-performance Low-cost Electrocatalysts for Overall Water Splitting. *J. Mater. Chem. A* 2017, 5, 7769-7775.

[S10] X. Y. Li, Z. G. Niu, J. Jiang and L. H. Ai, Cobalt Nanoparticles Embedded in Porous N-rich Carbon as an Efficient Bifunctional Electrocatalyst for Water Splitting. *J. Mater. Chem. A* 2016, 4, 3204-3209.

[S11] Yang, F. L.; Zhao, P. P.; Hua, X.; Luo, W.; Cheng, G. Z.; Xing W.; Chen, S. L.; A Cobalt-based Hybrid Electrocatalyst Derived from a Carbon Nanotube Inserted

Metal-Organic Framework for Efficient Water-Splitting. *J. Mater. Chem. A* 2016, 4, 16057-16063.

[S12] Meng, T.; Qin, J. W.; Wang, S. G.; Zhao, D.; Mao, B. G.; Cao, M. H.; In Situ Coupling of $Co_{0.85}Se$ and N-doped Carbon *via* One-Step Selenization of Metal-Organic Frameworks as a Trifunctional Catalyst for Overall Water Splitting and Zn-Air Batteries. *J. Mater. Chem. A* 2017, 5, 7001-7014.

[S13] Wang, J.; Zhong, H. X.; Wang, Z. L.; Meng, F. L.; Zhang, X. B. Integrated Three-Dimensional Carbon Paper/Carbon Tubes/Cobalt-Sulfide Sheets as an Efficient Electrode for Overall Water Splitting. *ACS Nano* 2016, 10, 2342-2348.

[S14] X. Zhang, H. M. Xu, X. X. Li, Y. Y. Li, T. B. Yang, and Y. Y. Liang. Facile Synthesis of Nickel-Iron/Nanocarbon Hybrids as Advanced Electrocatalysts for Efficient Water Splitting. *ACS Catal.* 2016, 6, 580-588.